J. Fluid Mech. (2012), *vol.* 701, *pp.* 251–277. © Cambridge University Press 2012
doi:10.1017/jfm.2012.156

Oscillatory sensitivity patterns for global modes in wakes

Outi Tammisola†

Linné Flow Centre, KTH Mechanics, Royal Institute of Technology, S-100 44 Stockholm, Sweden

(Received 20 May 2011; revised 12 December 2011; accepted 26 March 2012;
first published online 18 May 2012)

Globally unstable wakes with co-flow at intermediate Reynolds numbers are studied, to quantify important spatial regions for the development and control of the global instability. One region of high structural sensitivity is found close to the inlet for all wakes, in agreement with previous findings for cylinder wakes. A second, elongated region of high structural sensitivity is seen downstream of the first one for unconfined wakes at $Re = 400$. When base-flow modifications are considered, a spatially oscillating sensitivity pattern is found inside the downstream high-structural-sensitivity region. This implies that the same change in the base flow can either destabilize or stabilize the flow, depending on the exact position where it is applied. It is shown that the sensitivity pattern remains unchanged for different choices of streamwise boundary conditions and numerical resolution. The actual base-flow is modified in selected configurations, and the linear global modes recomputed. It is confirmed that the linear global eigenvalues move according to the predicted sensitivity pattern for small-amplitude base-flow modifications, for which the theory applies. We also look at the implications of a small control cylinder for the flow. Only the upstream high-sensitivity region proves to be robust in terms of control, but one should be careful not to disturb the flow in the downstream high-sensitivity region, in order to achieve control. The findings can have direct implications for the numerical resolution requirements for wakes at higher Reynolds numbers. Furthermore, they provide one more possible explanation for why confined wakes have a more narrow frequency spectrum than unconfined wakes.

Key words: absolute/convective instability, instability control, wakes

1. Introduction

Above a critical Reynolds number (Re), wake flows are susceptible to self-sustained oscillations at a distinct frequency. A well-known example is the von Kármán vortex street for a flow past a solid cylinder, which beats at the non-dimensional frequency (Strouhal number) $St \approx 0.2$, and appears for $Re \approx 47$–49 based on the cylinder diameter and inflow velocity (Williamson 1996; Zdravkovich 1997; Fey, König & Eckelmann 1998). The critical Reynolds number coincides with the value of Re for which a global eigenmode for the linearized Navier–Stokes equations first becomes unstable, and the frequency of oscillation at the onset is close to the frequency of the

† Present address: Department of Engineering, University of Cambridge, Cambridge CB2 1PZ, UK. Email address for correspondence: olot2@cam.ac.uk

https://doi.org/10.1017/jfm.2012.156 Published online by Cambridge University Press

linear mode (Zebib 1987). On the other hand, as long as the growth rates for all linear eigenmodes are negative, no self-sustained oscillations occur.

Following the success of global linear stability theory for the cylinder flow, new theories have emerged on the self-sustained oscillations and their control, based on the global linear eigenmodes and the eigenmodes of the adjoint linearized Navier–Stokes equations. The aim of these theories is to determine the precise spatial location where the instability has its origin and can be controlled by different means of forcing or perturbations. If such a localized region can be identified, it is sometimes called the *wavemaker*.

The sensitivity of the growth rate and frequency of the global mode to structural changes in the momentum equations was examined by Giannetti & Luchini (2007). A goal was to determine regions where a small control cylinder should be placed in order to have a maximal effect on the stability, and hopefully stabilize the global mode. This would then theoretically explain the stabilizing effect observed in experiments of Strykowski & Sreenivasan (1990). The theoretical approach was taken further by Marquet, Sipp & Jacquin (2008) by introducing the sensitivity to (arbitrary) base-flow modifications, and the sensitivity to a static volume forcing. Further, they modelled a small control cylinder as a volume force, taking into account the effect of this force on the base flow, and their results compared favourably to the experimental regions where vortex shedding was suppressed (Strykowski & Sreenivasan 1990). In Pralits, Brandt & Giannetti (2010), both the effects on the base flow and the disturbance were modelled for a rotating cylinder. When presenting this chronological flow of discoveries, it should also be noted that an equivalent expression specifically for the sensitivity for a control cylinder was presented earlier in the sometimes overlooked work of Hill (1992).

Furthermore, cylinders confined in a channel have been studied in direct numerical simulation (DNS) by e.g. Richter & Naudascher (1976), who found that confinement increased the level of lift fluctuations and made the frequency spectrum more concentrated around the dominant frequency, especially at higher Reynolds numbers ($Re > 750$). More well-defined frequency peaks for half-confined cylinder wakes have also been reported by Bearman & Zdravkovich (1978) at $Re = 350$.

The present work deals with a slightly different wake flow, the co-flow wake. Here, one inner flow stream with low velocity meets and mixes with two outer flow streams with high velocity (see the inlet profile in figure 1, and base flows in figure 2*a–c*). The strength of the wake is determined by the shear ratio between inner and outer flows at the inlet. Viscous spatially developing co-flow wakes have been analysed by linear global modes in Tammisola *et al.* (2011), and by a local weakly non-parallel analysis of the same base flows in Juniper, Tammisola & Lundell (2011). In particular, both works addressed the effect of confinement on the global stability of co-flow wakes at intermediate wake Reynolds numbers ($Re = 100$–400). It was found that confinement was globally stabilizing, partly due to a decreasing wake length and partly since the boundary layers at the walls made the wake less locally unstable. At $Re = 400$, the shear ratios at the onset of global instability for unconfined and confined wakes were practically equal, and this was attributed to a similar base-flow development in the upstream region ($x < 50$). On the other hand, previous local analyses have shown that confinement can have a destabilizing effect through saddle-point interaction (Juniper 2006; Rees & Juniper 2010), especially at high Reynolds numbers. This effect was also visible in the local analysis of the spatially developing wakes at moderate Re, but overshadowed by other effects (Juniper *et al.* 2011).

https://doi.org/10.1017/jfm.2012.156 Published online by Cambridge University Press

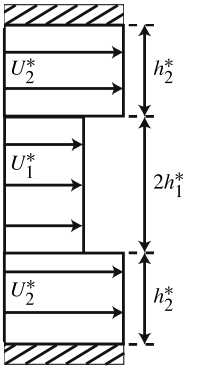


FIGURE 1. The inlet profile with dimensional parameters.

The present work was initiated to see whether the equal stability limits for confined and unconfined wakes at $Re \approx 400$ are due to similar base flows in the upstream region. It would then seem natural to expect that the sensitivity characteristics of both flows are very similar, and identify the same region upstream that dictates the instability dynamics. The findings will show that although the hypothesis is not completely wrong, the dynamics of the unconfined wakes in Tammisola *et al.* (2011) are fundamentally different from the confined ones, and show surprising features.

The manuscript is organized as follows: having provided the relevant background in § 1, the mathematical description of the sensitivities is given in § 2, the wavemakers and sensitivities to generic base-flow modifications are shown in § 3, with further verification in § 4 (with numerical details left to appendix A). The sensitivity to a volume force and its application for a small control cylinder are presented in § 5. The results are discussed in § 6, and conclusions drawn in § 7. Further, results for a co-flow wake with a slightly different geometry are shown in appendix B, and an expression for the volume force generated by the small cylinder derived in appendix C.

2. Definitions of parameters and sensitivity measures

The problem is non-dimensionalized based on the inlet profile, and the dimensional quantities denoted by a tilde. The parameter definitions are as follows (see figure 1):

(i) confinement parameter h

$$h = \frac{\tilde{h}_2}{\tilde{h}_1}; \tag{2.1}$$

(ii) Reynolds number Re

$$Re = \frac{\tilde{U}_2 \tilde{h}_1}{\tilde{\nu}}, \tag{2.2}$$

where $\tilde{\nu}$ is the kinematic viscosity of the fluids;

(iii) shear ratio describing the strength of the shear between the fluids at the inlet compared to their momentum

$$\Lambda = \frac{(\tilde{U}_1 - \tilde{U}_2)}{(\tilde{U}_1 + \tilde{U}_2)}. \tag{2.3}$$

https://doi.org/10.1017/jfm.2012.156 Published online by Cambridge University Press

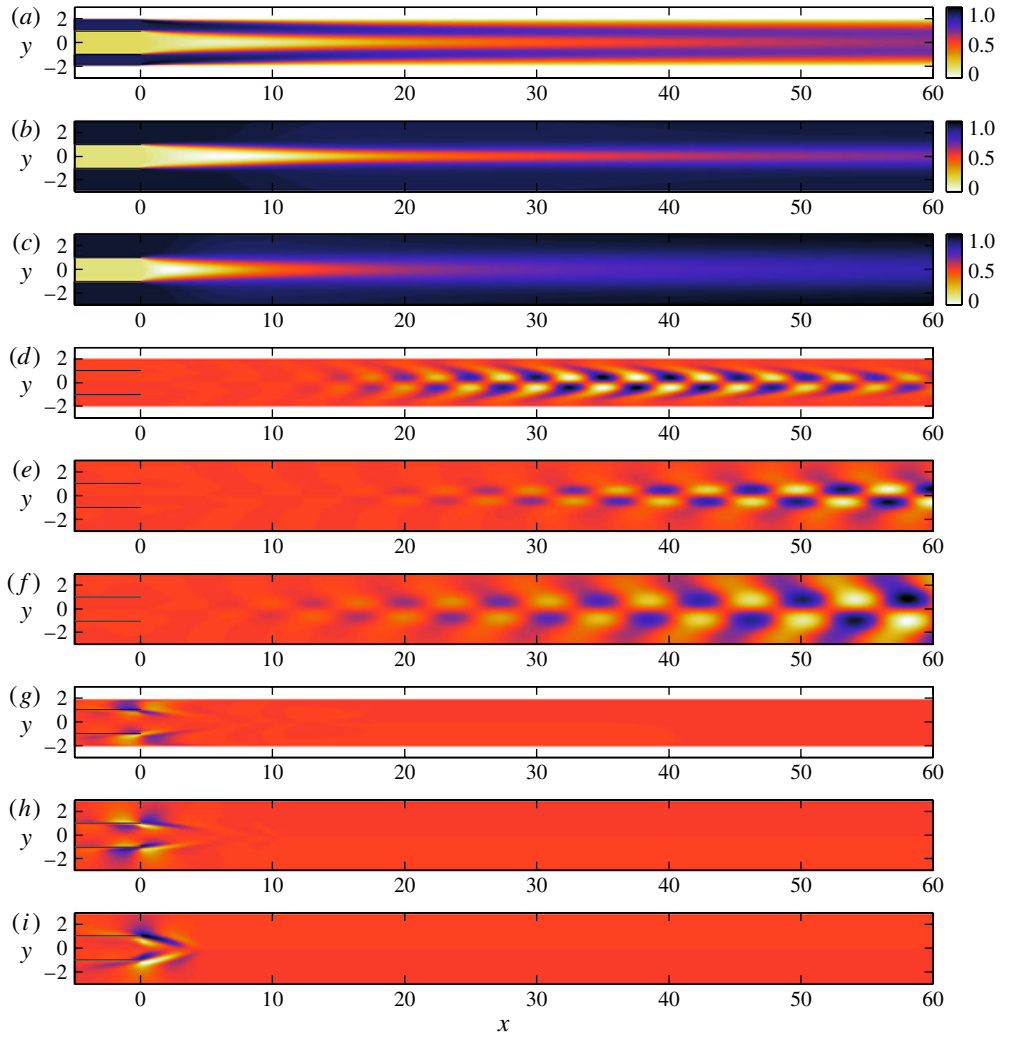


FIGURE 2. (Colour online available at journals.cambridge.org/flm) The base flows, and direct and adjoint global modes, used to compute sensitivities for the three wakes under study. Note that the computational domain extends far beyond the axis limits in all directions. The purpose of the region $x < 0$, where the flow streams are separated by a splitter plate (black line), is purely to let the direct and adjoint global modes decay smoothly instead of setting them to zero at the flow inlet (the concept is further described in appendix A). Streamwise velocity of the base flow: (*a*) $h = 1$, $Re = 398$; (*b*) $h = 9$, $Re = 398$; (*c*) $h = 9$, $Re = 100$. Leading direct global mode, real part of the streamwise velocity: (*d*) $h = 1$, $Re = 398$; (*e*) $h = 9$, $Re = 398$; (*f*) $h = 9$, $Re = 100$. Leading adjoint global mode, real part of the streamwise velocity: (*h*) $h = 1$, $Re = 398$; (*g*) $h = 9$, $Re = 398$; (*i*) $h = 9$, $Re = 100$.

The inverse of the shear ratio, Λ^{-1}, is more often used here, and a high absolute value means a strong co-flow (base bleed); for example $\Lambda^{-1} = -1.5$ means $\tilde{U}_1/\tilde{U}_2 = 0.2$, $\Lambda^{-1} = -1$ means $\tilde{U}_1/\tilde{U}_2 = 0$ (no co-flow).

The base flow (U, V, P) is obtained by solving the steady Navier–Stokes (N–S) equations. Other governing equations that are solved are the following.

https://doi.org/10.1017/jfm.2012.156 Published online by Cambridge University Press

(*a*) The linear global system

$$-\frac{\partial u}{\partial t} - U\frac{\partial u}{\partial x} - V\frac{\partial u}{\partial y} - u\frac{\partial U}{\partial x} - v\frac{\partial U}{\partial y} - \frac{\partial p}{\partial x} + \frac{1}{Re}\left(\frac{\partial^2 u}{\partial x^2} + \frac{\partial^2 u}{\partial y^2}\right) = 0, \quad (2.4)$$

$$-\frac{\partial v}{\partial t} - U\frac{\partial v}{\partial x} - V\frac{\partial v}{\partial y} - u\frac{\partial V}{\partial x} - v\frac{\partial V}{\partial y} - \frac{\partial p}{\partial y} + \frac{1}{Re}\left(\frac{\partial^2 v}{\partial x^2} + \frac{\partial^2 v}{\partial y^2}\right) = 0, \quad (2.5)$$

$$\frac{\partial u}{\partial x} + \frac{\partial v}{\partial y} = 0, \quad (2.6)$$

where (u, v, p) is the disturbance. The global-mode ansatz is made in these equations, and they are solved with respect to the complex eigenvalue ω:

$$[u, v, p] = [\hat{u}(x, y), \hat{v}(x, y), \hat{p}(x, y)]\mathrm{e}^{-\mathrm{i}\omega t}. \quad (2.7)$$

(*b*) The adjoint linear global system

$$-\frac{\partial u^+}{\partial t} - U\frac{\partial u^+}{\partial x} - V\frac{\partial u^+}{\partial y} + u^+\frac{\partial U}{\partial x} + v^+\frac{\partial V}{\partial x} + \frac{\partial p^+}{\partial x} - \frac{1}{Re}\left(\frac{\partial^2 u^+}{\partial x^2} + \frac{\partial^2 u^+}{\partial y^2}\right) = 0, \quad (2.8)$$

$$-\frac{\partial v^+}{\partial t} - U\frac{\partial v^+}{\partial x} - V\frac{\partial v^+}{\partial y} + u^+\frac{\partial U}{\partial y} + v^+\frac{\partial V}{\partial y} + \frac{\partial p^+}{\partial y} - \frac{1}{Re}\left(\frac{\partial^2 v^+}{\partial x^2} + \frac{\partial^2 v^+}{\partial y^2}\right) = 0, \quad (2.9)$$

$$\frac{\partial u^+}{\partial x} + \frac{\partial v^+}{\partial y} = 0, \quad (2.10)$$

where (u^+, v^+, p^+) is the adjoint disturbance. The global-mode ansatz is made in these equations also, and they are solved with respect to the complex eigenvalue ω^+:

$$[u^+, v^+, p^+] = [\hat{u}^+(x, y), \hat{v}^+(x, y), \hat{p}^+(x, y)]\mathrm{e}^{-\mathrm{i}\omega^+ t}. \quad (2.11)$$

In the continuous formulation (with correct boundary conditions for the adjoint problem), it can be shown that $\omega^+ = \omega^*$, where the star denotes complex conjugate. Hence, the comparison of adjoint and direct eigenvalues serves as a nice resolution check of both the direct and adjoint problems.

The adjoint needs to fulfil the following normalization condition, for the sensitivity expressions presented here to be valid:

$$\int u^{+*}u = 1. \quad (2.12)$$

The numerical solution and boundary conditions are briefly described in appendix A.

The sensitivity of the eigenvalue to modifications of a quantity ϕ is defined as

$$\delta\omega = \int \gamma^*(x, y)\delta\phi(x, y)\,\mathrm{d}x\,\mathrm{d}y, \quad (2.13)$$

where γ is a sensitivity distribution. In other words, by taking the inner product of the modification (e.g. base-flow changes) and the corresponding sensitivity function (e.g. sensitivity to base-flow modifications), one obtains the change in the eigenvalue. Observe that the expression above is complex-valued, and that the changes in growth rate and frequency can be treated separately.

https://doi.org/10.1017/jfm.2012.156 Published online by Cambridge University Press

The wavemakers presented in this paper are described by the following equations.

(i) The general structural sensitivity (Giannetti & Luchini 2007). The upper bound of the sensitivity to perturbations in the u-momentum equation (2.4) is obtained from

$$S(x, y) = |\hat{u}(x, y)||\hat{u}^{+}(x, y)|. \tag{2.14}$$

This means that $|\delta\omega| \leqslant S(x, y)A$, where A is the perturbation amplitude.

(ii) The sensitivity to generic base-flow modifications (Marquet *et al.* 2008), where the modified base flow is not necessarily a solution to steady Navier–Stokes equations:

(a) for the streamwise component

$$S_U(x, y) = -\frac{\partial \hat{u}^*}{\partial x}\hat{u}^{+} - \frac{\partial \hat{v}^*}{\partial x}\hat{v}^{+} + \frac{\partial \hat{u}^{+}}{\partial x}\hat{u}^* + \frac{\partial \hat{u}^{+}}{\partial y}\hat{v}^*, \tag{2.15}$$

(b) for the vertical component

$$S_V(x, y) = -\frac{\partial \hat{u}^*}{\partial y}\hat{u}^{+} - \frac{\partial \hat{v}^*}{\partial y}\hat{v}^{+} + \frac{\partial \hat{v}^{+}}{\partial x}\hat{u}^* + \frac{\partial \hat{v}^{+}}{\partial y}\hat{v}^*. \tag{2.16}$$

Note that both (ii$a$) and (ii$b$) are complex quantities, where the sensitivity of the growth rate is obtained from the real part and the sensitivity of the frequency from the imaginary part (where the latter differs from Marquet *et al.* 2008 due to a different definition of the eigenvalue).

The expressions (2.15) and (2.16) can be further divided into the sensitivity to changes in the base-flow advection (first two terms) and changes in the energy extraction from base-flow gradients ('production', second two terms). Here, we define the following expressions for the growth rate sensitivity:

$$S_{adv} = \sqrt{S_{U,adv}^2 + S_{V,adv}^2}, \tag{2.17}$$

and

$$S_{prod} = \sqrt{S_{U,prod}^2 + S_{V,prod}^2}, \tag{2.18}$$

where

$$S_{U,adv} = \mathrm{Re}\left[-\frac{\partial \hat{u}^*}{\partial x}\hat{u}^{+} - \frac{\partial \hat{v}^*}{\partial x}\hat{v}^*\right], \tag{2.19}$$

$$S_{U,prod} = \mathrm{Re}\left[\frac{\partial \hat{u}^{+}}{\partial x}\hat{u}^* + \frac{\partial \hat{u}^{+}}{\partial y}\hat{v}^*\right], \tag{2.20}$$

$$S_{V,adv} = \mathrm{Re}\left[-\frac{\partial \hat{u}^*}{\partial y}\hat{u}^{+} - \frac{\partial \hat{v}^*}{\partial y}\hat{v}^{+}\right], \tag{2.21}$$

$$S_{V,prod} = \mathrm{Re}\left[\frac{\partial \hat{v}^{+}}{\partial x}\hat{u}^* + \frac{\partial \hat{v}^{+}}{\partial y}\hat{v}^*\right]. \tag{2.22}$$

(iii) The sensitivity to a steady and unsteady volume force (Pralits *et al.* 2010).

The sensitivity to a steady volume force is given by

$$S_F = U^{+}, \tag{2.23}$$

https://doi.org/10.1017/jfm.2012.156 Published online by Cambridge University Press

where U^+ is the solution to the adjoint base-flow equations

$$-U_j\frac{\partial U_i^+}{\partial x_j}+U_j^+\frac{\partial U_j}{\partial x_i}-\frac{\partial P^+}{\partial x_i}-\frac{1}{Re}\left(\frac{\partial U_i^+}{\partial x_j\partial x_j}\right)=-\frac{\partial \hat{u}_j^*}{\partial x_i}\hat{u}_j^+ +\frac{\partial \hat{u}_i^+}{\partial x_j}\hat{u}_j. \tag{2.24}$$

Further, to model a small control cylinder we assume a force proportional to the velocity: a steady force $F_i=\delta(x-x_0)(y-y_0)M_{ij}u_j$, and an unsteady force $f=\delta(x-x_0)(y-y_0)m_{ij}u_j$. The matrices $M_{ij}=M_{ij}(x,y)$ and $m_{ij}=m_{ij}(x,y)$ are related to the specific drag model for the small cylinder, and are given in appendix C for the model used in the present work.

The sensitivity to the small control cylinder is then given by (Pralits *et al.* 2010)

$$\delta\omega=U_i^+M_{ij}U_j+u_i^+m_{ij}u_j. \tag{2.25}$$

3. General structural sensitivities of co-flow wakes

Here, we present sensitivity distributions for the most unstable mode of three wakes: high-Reynolds-number confined ($Re=398$, $h=1$), high-Reynolds-number unconfined ($Re=398$, $h=9$), and low-Reynolds-number unconfined ($Re=100$, $h=9$).

The wake base flows are shown in figure 2(*a–c*). At the wake inlet (at $x=0$) the inner stream has a low co-flow velocity of $U_2=0.14$ for all wakes, and the flow develops towards a parabolic profile downstream. For the unconfined wakes, there is a region of a slight reverse flow (with minimum velocity $U=-0.005$) around $x\approx 7$ and $x\approx 3$, respectively for high and low Reynolds number. The direct and adjoint eigenmodes used for computing sensitivity distributions are shown in figure 2(*d–i*). In all three cases, the amplitude distributions of the direct mode and its corresponding adjoint are different from each other, indicating streamwise non-normality; the eigenmode shown in figure 2(*e*) reaches its amplitude maximum at $x\approx 85$, far outside the figure frame. Note that only a representative part of each eigenfunction is shown – the actual computational domain is $L\times d_y=[-10,250]\times[0,10]$ (due to symmetry of the base flow, it is sufficient to use only upper half of the domain, and impose symmetry/antisymmetry for the mode at the centreline).

Now we move on to the sensitivity studies, which are the main topic of the present work. Only the upper halves of the sensitivity distributions are shown, since the symmetry of the base flow implies that they are symmetric around the centreline. The magnitude of the sensitivity for structural perturbations S (equation (2.14)) for each of the wakes is shown in figure 3. We begin with the confined wake.

For the confined wake (figure 3*a*), high amplitude of the structural sensitivity S is found in the region $0<x<10$. The maximum of the sensitivity lies around the shear layer, but the sensitivity also has a visible amplitude close to the wall, showing an effect of confinement. Apart from the confinement effect, this is similar to the wavemakers for cylinder wakes at slightly supercritical Reynolds numbers shown in the previous works (Giannetti & Luchini 2007; Pralits *et al.* 2010).

The structural sensitivity of the unconfined wake for the same Reynolds number is shown in figure 3(*b*). There is a similar high-sensitivity region close to the inlet, and the overall maximum of the sensitivity is at $x\approx 6.2$. However, a second region of high sensitivity appears downstream, and is extremely elongated with a maximum at $x\approx 20$. The second region also extends higher up in the outer flow; at $y=4$ the amplitude is still 0.03, i.e. 10 % of the total maximum amplitude of S. There are no additional sensitivity regions, and the sensitivity has no visible amplitude outside the figure frame shown. The same quantity for the unconfined wake at a lower Reynolds

https://doi.org/10.1017/jfm.2012.156 Published online by Cambridge University Press

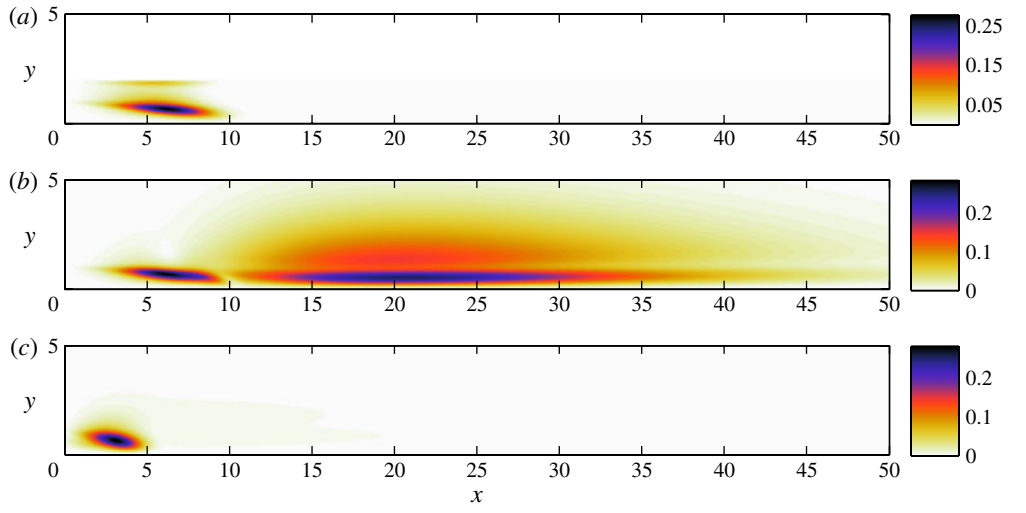


FIGURE 3. (Colour online) The structural sensitivity S for wakes: (a) $Re = 398$ and $h = 1$; (b) $Re = 398$ and $h = 9$; (c) $Re = 100$ and $h = 9$. The region $y > 0$ is shown; the sensitivity at $y < 0$ is the mirror image.

number (figure 3c) again shows only one sensitivity region. As one would expect, the sensitivity region is located closer to the inlet and down to the low-speed region close to the symmetry line, again in full agreement with cylinder wakes at slightly supercritical Reynolds numbers.

Now, we leave the arbitrary structural perturbations, and look specifically at how small perturbations of the base-flow field affect the stability. First, the sensitivity of the global-mode growth rate to generic modifications in the streamwise base-flow velocity is considered. We begin again with the confined wake (figure 4a). The growth rate is increased if the streamwise velocity is decreased in the lower part of the shear layer, and increased in the upper part. The effect is very intuitive, since both changes make the wake stronger, inside the region where the wavemaker is strong (figure 3a). In addition, the growth rate increases if the velocity is increased close to the wall, i.e. if the boundary layer near the wall is removed, in agreement with Juniper *et al.* (2011).

For the unconfined wake (figure 4b), the base-flow modification acts in a more curious way. There are similar structures upstream as in the confined case, but the sensitivity is clearly stronger inside the downstream located wavemaker region of figure 3(b). Furthermore, inside this region, the sensitivity oscillates between positive and negative values, with a similar wavelength as the one for the direct eigenmode. This means that if we introduce a small base-flow modification for example at the centreline ($y = 0$), at $x = 17$ or $x = 23$, we get an increased growth rate, but when doing the same at $x = 21$ or $x = 27$, the growth rate decreases. At the low Reynolds number but unconfined wake (figure 4c), the sensitivity is again concentrated close to the inlet, although some traces of a wave-like sensitivity at a low amplitude are seen downstream. More extensive parameter variations have shown that the change between the two states is continuous, as the Reynolds number increases. The sensitivity to base-flow modifications for unconfined wakes is surprising and counterintuitive, unlike the confined wakes. The rest of this paper exclusively investigates this phenomenon.

https://doi.org/10.1017/jfm.2012.156 Published online by Cambridge University Press

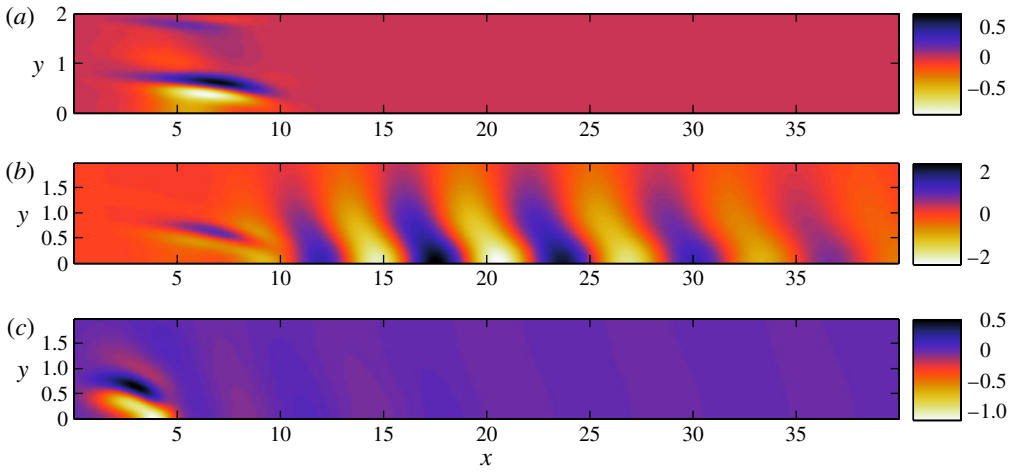


FIGURE 4. (Colour online) The sensitivity of the growth rate to generic modifications in streamwise base-flow velocity (Re[S_U]): (*a*) $Re = 398$ and $h = 1$; (*b*) $Re = 398$ and $h = 9$; (*c*) $Re = 100$ and $h = 9$. Note that the axis limits differ from the ones in figure 3. The region $y > 0$ is shown; the sensitivity at $y < 0$ is the mirror image.

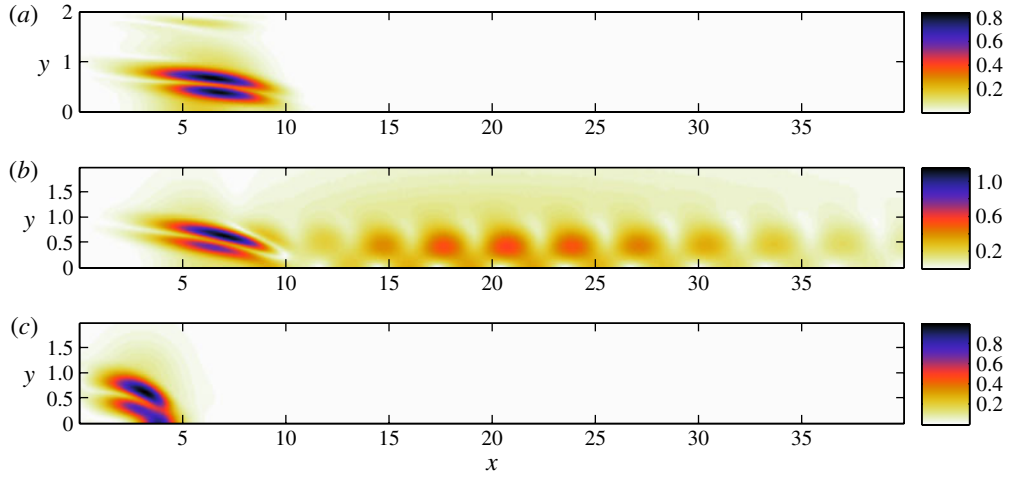


FIGURE 5. (Colour online) The magnitude of the sensitivity of the growth rate to generic base-flow modifications, production part S_{prod}: (*a*) $Re = 398$ and $h = 1$; (*b*) $Re = 398$ and $h = 9$; (*c*) $Re = 100$ and $h = 9$. The region $y > 0$ is shown; the sensitivity at $y < 0$ is the mirror image.

Next, we divide the sensitivity to base-flow modifications into the sensitivity to changes in production and changes in advection. The former is shown for all wakes in figure 5. From figure 5(*b*) it is seen that the production part of the unconfined wake is still more localized in the upstream wavemaker region, and does not substantially differ from that of the confined wake at the same Reynolds number in figure 5(*a*). Figure 6(*b*) reveals that the oscillating sensitivity is mostly due to changes in advection (note that the colourmaps in figures 5*b* and 6*b* are different). This shows that the

https://doi.org/10.1017/jfm.2012.156 Published online by Cambridge University Press

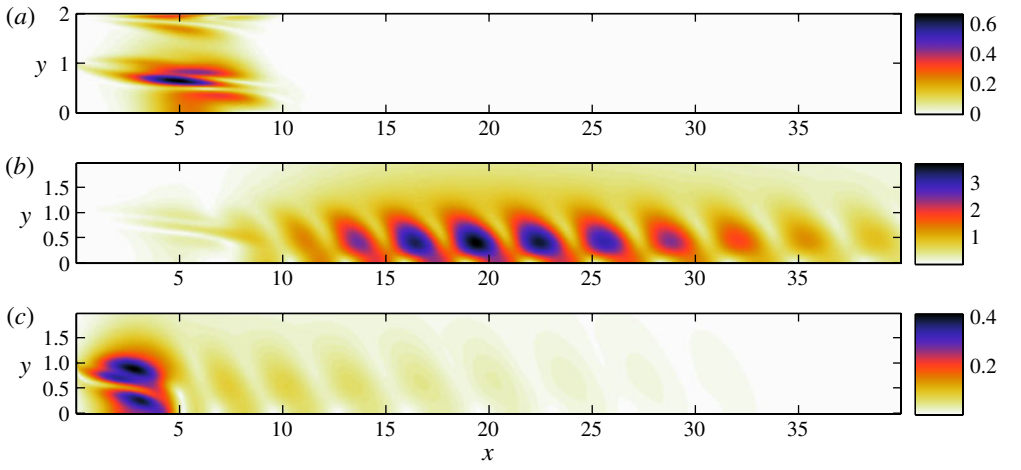


FIGURE 6. (Colour online) The magnitude of the sensitivity of the growth rate to generic base-flow modifications, advection part S_{adv}: (*a*) $Re = 398$ and $h = 1$; (*b*) $Re = 398$ and $h = 9$; (*c*) $Re = 100$ and $h = 9$. The region $y > 0$ is shown; the sensitivity at $y < 0$ is the mirror image.

main source of the instability still comes from the upstream wavemaker, while the downstream wavemaker acts to either heal the symptoms or make matters worse, by letting the disturbance be convected downstream in different amounts. Being the dominant contributor to the sensitivity to base-flow modifications, the downstream wavemaker should in any case not be overlooked.

4. Verification of the oscillating sensitivity pattern of the unconfined wake at $Re = 398$

As the Reynolds number increases, the co-flow wake becomes increasingly parallel and therefore the global modes are more non-normal (Chomaz 2005). It is thus essential to verify that the oscillating sensitivity is not a product of insufficient resolution, boundary conditions or even a particular numerical discretization method. Both the wavemaker and the sensitivity to base-flow modifications of the unconfined wake have been verified by changing the method for computing the base flow and stability, the resolution, and the location of the boundaries of the computational domain. The whole pattern remained unchanged, and in particular, the phase and location of maximal sensitivity for the same wake did not change. Modelling the region before the wake inlet more carefully has also been tested, including a rounded-edge splitter plate with a finite thickness, where boundary layers are allowed to develop. This naturally changes the base flow, and therefore the sensitivities, but the oscillating pattern remains, and in fact has an even higher amplitude in this case. The results of the numerical tests will be summarized in appendix A, and the results for a round-edged plate with boundary layers in appendix B.

It is easy to test whether the adjoint-based sensitivity distributions are the true ones for a certain linear global mode problem, with prescribed boundary conditions. This can be done by applying a series of localized base-flow modifications to the problem, and recalculating the direct eigenvalues. Here, the V-component of the base flow is

https://doi.org/10.1017/jfm.2012.156 Published online by Cambridge University Press

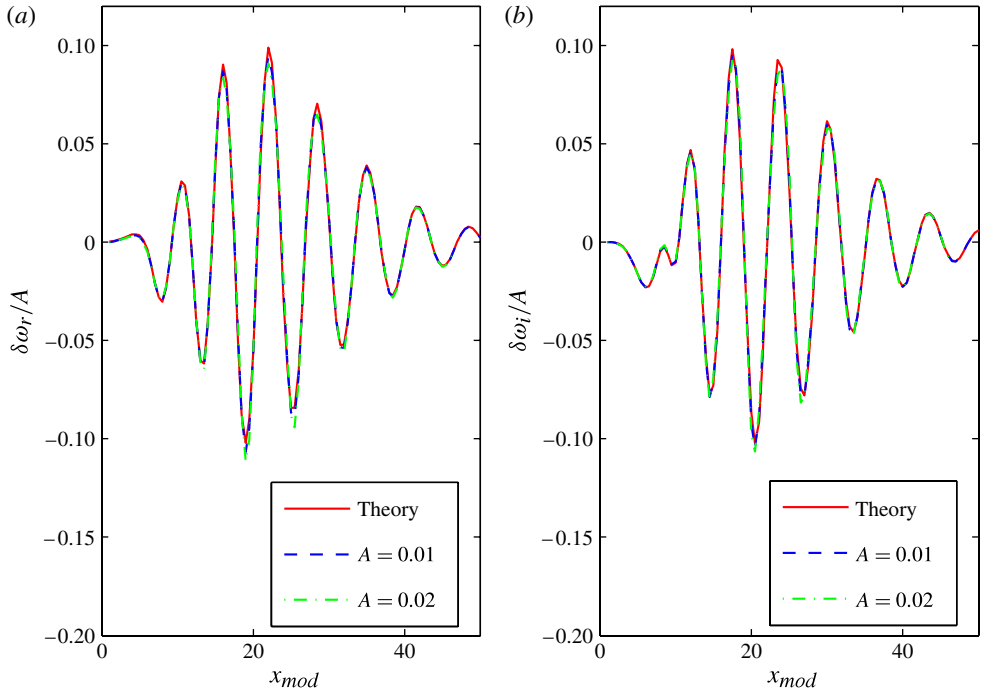


FIGURE 7. (Colour online) (*a*) The frequency and (*b*) the growth rate of the most unstable eigenvalue with modifications of different amplitude along the line $y = 0.5$ (varying x_{mod}), normalized with the amplitude: the theoretical curve obtained directly from the sensitivity distributions (solid); global modes recomputed with $A = 0.01$ (− −); global modes recomputed with $A = 0.02$ (− · −).

altered by superimposing a Gaussian centred around the line $y = 0.5$:

$$V_{mod} = V + A \exp[-100\,(x - x_{mod})^2 - 100\,(y - 0.5)^2]. \tag{4.1}$$

The derivatives of V are altered accordingly. The amplitude A of the base-flow modification needs to be small enough for the linear theory to be valid, and the appropriate level is found by trial and error.

The theoretical change in the eigenvalue, when such a modification is applied, is obtained from the sensitivity distributions by integrating the product of $(V_{mod} - V)$ and the complex conjugate of the sensitivity distribution over the computational domain.

These theoretical curves with $A = 1$ as a function of x_{mod} are shown with solid lines in figures 7(*a*) (growth rate part) and 7(*b*) (frequency part). The other line styles represent changes in the eigenvalue that are obtained by applying the base-flow modification in the direct problem and recomputing the eigenvalues. Different maximum amplitudes of the Gaussian are chosen: $A = 0.01$ and $A = 0.02$ (10 % of the maximum amplitude for V and ≈2 % of the maximum amplitude for U), and and the result is normalized with A. The curves with the two small amplitudes collapse nicely with the theoretical curve.

These results show that the sensitivity is inherent to the physical problem, and is not related to errors in the numerical or analytical solution of the problem.

https://doi.org/10.1017/jfm.2012.156 Published online by Cambridge University Press

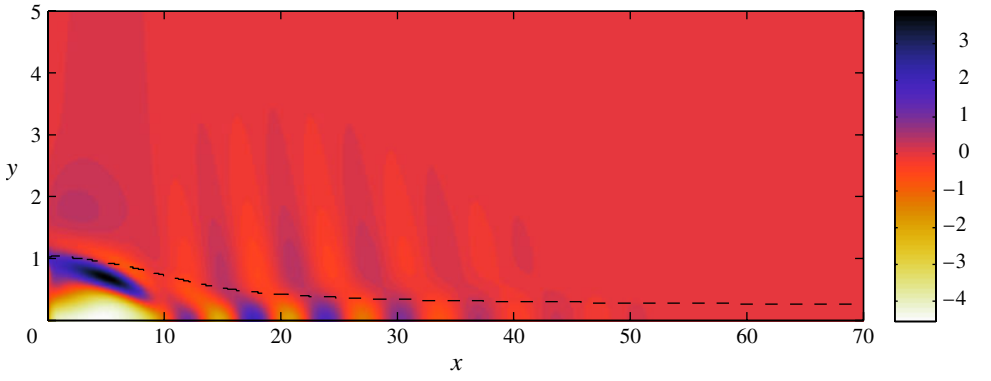


FIGURE 8. (Colour online) Sensitivity to a steady volume force in the streamwise direction (positive forcing direction aligned with unit vector [1, 0]). The streamline starting between the two flow streams at the inlet is shown with a dashed line. The region $y > 0$ is shown; the sensitivity at $y < 0$ is the mirror image.

5. Sensitivity to a volume force and implications for passive control

The response to local base-flow modifications was examined previously. This provides insight into where local changes of the base-flow profile are most efficient. However, when a real passive control is applied locally, it can have a global effect through transport and production by the base flow. In other words, the modified base-flow field will still satisfy Navier–Stokes equations.

Next, passive control is modelled as a steady volume force (2.23), so that the modified base flow satisfies the steady Navier–Stokes equations. The resulting growth rate sensitivity distribution for a volume force applied in the streamwise direction is seen in figure 8. By following the streamline starting between the outer and inner flow at the inlet (dashed line), it is obvious that shear below this line controls the flow. The growth rate of the global mode increases if the flow is accelerated in the upper part of this 'inner flow', and decelerated in the lower part. Further downstream, the oscillating pattern is visible, but has a lower amplitude. Observe that this does not contradict the previous results, since the present analysis can take into account non-local changes, such as a modification of the wake length due to local changes in the upstream flow.

5.1. *Sensitivity to a small control cylinder*

Next, a small control cylinder is modelled as a steady and unsteady volume force, following Pralits *et al.* (2010) (and equivalent to Hill 1992). Here, Re_c is the Reynolds number of the small cylinder. Pralits *et al.* (2010) modelled the force using the Lamb–Oseen drag coefficient for a cylinder valid for $Re_c \ll 1$, and Hill (1992) adjusted constants in a low-Reynolds-number drag coefficient model. Here, we use the model of Imai (1951) that is shown to give good agreement with experiments for $5 < Re_c < 100$ in Zdravkovich (1997):

$$C_D = \left(0.707 + \frac{3.42}{\sqrt{Re_c}}\right)^2. \tag{5.1}$$

Note that the steady and linearized oscillatory parts of this force are derived in appendix C. The lift on the control cylinder due to local shear is assumed to be negligible. Estimates based on the low-Reynolds-number lift model of Filon (1926) and maximal circulation over a cylinder with diameter $D = 0.02$ in the base flow

https://doi.org/10.1017/jfm.2012.156 Published online by Cambridge University Press

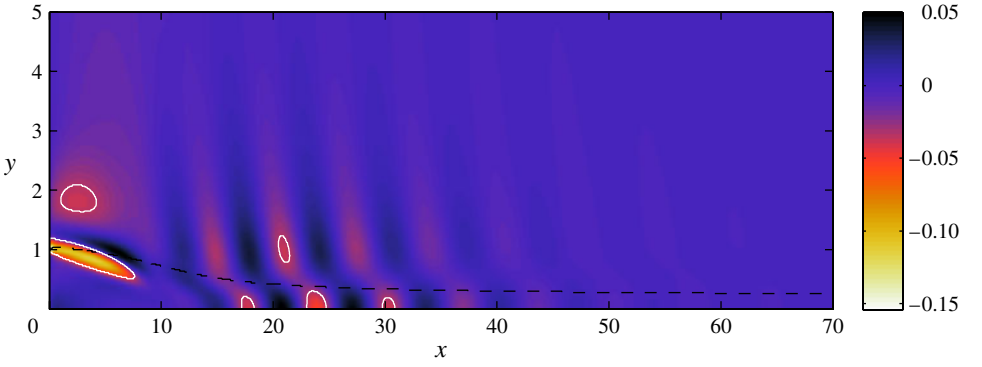


FIGURE 9. (Colour online) Sensitivity to a control cylinder of diameter 0.04. Light regions imply a reduced growth rate of the global mode, and dark regions an increased growth rate. The white contours surround the regions where the model predicts stabilization. The streamline starting between the two flow streams at the inlet is shown with a dashed line. The region $y > 0$ is shown; the sensitivity at $y < 0$ is the mirror image.

indicated that the lift on the control cylinder was two orders of magnitude less than the drag.

The predicted change in the growth rate of the global mode, when a cylinder with diameter 0.04 is inserted at different positions in the flow domain, is shown in figure 9. The colourscale gives the magnitude and direction of the change (positive or negative), as a function of the position of the control cylinder. First, we note that this change has mainly the opposite sign compared to the sensitivity to a steady volume forcing in figure 8. This is due to the fact that there is no reverse flow. Hence, the cylinder decelerates the flow everywhere, corresponding to a negative volume force. The next observation is that the forcing with a control cylinder is more efficient in regions with a high base-flow velocity, since it results in larger velocity difference and therefore a larger drag. The significance of the outer flow is somewhat increased in figure 9 compared to figure 8, and the dominant white region close to the centreline in figure 8 is neither stabilizing nor destabilizing for the control cylinder in figure 9.

5.2. *Global stability with insertion of the control cylinder*

Finally, we turn to the physical implications for the global stability as a whole. The boundaries of the regions where the control cylinder is supposed to stabilize this particular global mode (so that $\omega_i \leqslant 0$) are indicated by the white contours in figure 9. We now investigate the actual global mode problem, where the base flow and stability are recomputed with the small cylinder included. In Tammisola *et al.* (2011) it was shown that the stability for converged linear global modes matches exactly the stability limits seen in direct numerical simulations for co-flow wakes.

In the following, the control cylinder is inserted at a chosen position $x = x_{cyl}$, $y = y_{cyl}$ in the global mode computation. We start by investigating the strongest sensitivity region close to the inlet, and follow the line $y_{cyl} = 1.03$, for $0 < x_{cyl} < 5$. The computations show that with this position of the control cylinder, all global modes are stabilized. An example spectrum for $x_{cyl} = 1$, $y_{cyl} = 1.03$ is shown in figure 10(*a*), compared to the original spectrum. Thus, the flow can be controlled inside the stabilizing region found close to the inlet.

https://doi.org/10.1017/jfm.2012.156 Published online by Cambridge University Press

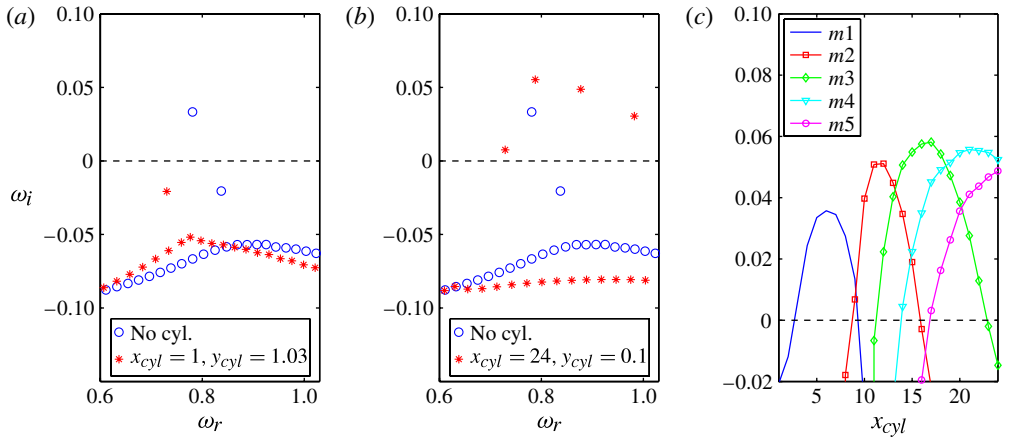


FIGURE 10. (Colour online) A cylinder with diameter $D = 0.04$ included in the base flow and gl(a)obal-mode computations: spectra with a cylinder at $x_{cyl} = 1$, $y_{cyl} = 1.03$ compared to the spectra without a control cylinder; (b) as (a) but at $x_{cyl} = 24$, $y_{cyl} = 0.1$; (c) the growth rate of the most unstable mode as a function of x_{cyl}, when $y_{cyl} = 1.03$.

Now, we insert the cylinder inside one of the smaller regions downstream, where the cylinder is also predicted to stabilize the flow (i.e. $\omega_i < 0$): at $x_{cyl} = 24$, $y_{cyl} = 0.1$. The spectrum (figure 10b) has changed completely, and now contains four unstable modes instead of one. Following the global mode with different x_{cyl} along the line $y_{cyl} = 1.03$ (figure 10c) reveals that a second mode becomes unstable when $x_{cyl} \approx 9$, and soon after this, the original mode stabilizes. A third mode becomes unstable at $x_{cyl} \approx 12$, while the second mode stabilizes at $x_{cyl} \approx 16$. This development continues with several modes. Each individual mode also increases in frequency with increasing x_{cyl}, and thus forms an arch in the spectrum with increasing x_{cyl}.

This mode switching pattern also results in oscillation of the mode growth rate. This oscillation should not be confused with the oscillatory pattern for one single mode predicted in figure 9. The force exerted by the cylinder is too large to be captured by the theory, where infinitesimal modification was assumed, and therefore the change in the growth rate predicted from figure 9 fails to be valid. To prove that the force from the cylinder is indeed too large, the test should be repeated with smaller and smaller cylinders until the theory is valid.

Since the discretization of smaller and smaller cylinders would become increasingly challenging for the numerical method, a test is performed by imposing the volume force from the model of Imai (1951) corresponding to inserting a cylinder with diameter 0.04 into the base-flow and global-mode computations, respectively (using the expressions derived in appendix C). The spectrum for a cylinder with diameter 0.04 inserted into the flow at $x = 24$, $y = 0.1$ was shown in figure 9(b). The spectrum with a volume force (according to the model of Imai 1951) applied at the same position is shown in figure 11(a). The spectrum is merely qualitatively similar to figure 9(b), showing that the cylinder model designed for uniform-velocity flows is only approximately valid for spatially developing flows. However, both spectra show a similar destabilization of several modes. We denote the amplitude of the volume force representing this cylinder by F_0. Now, the test is repeated with the same force distribution, but with a scaled amplitude F. The resulting growth rates of the leading

https://doi.org/10.1017/jfm.2012.156 Published online by Cambridge University Press

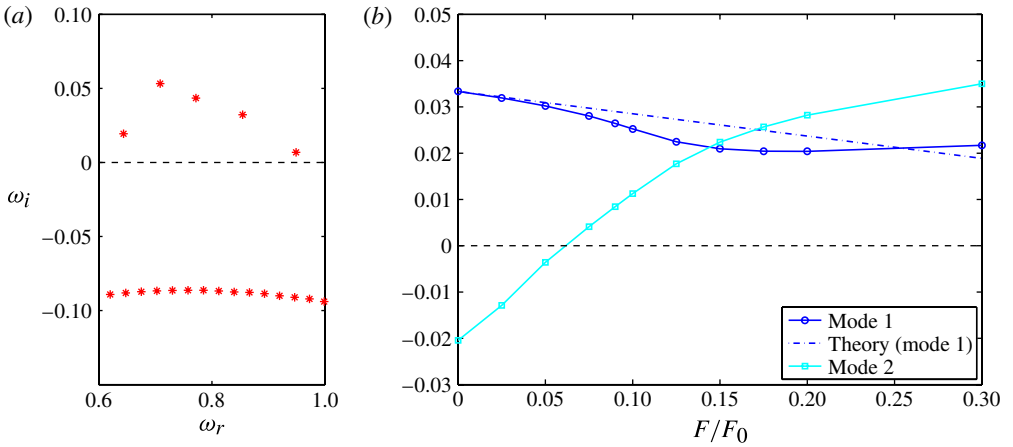


FIGURE 11. (Colour online) Force according to the model of Imai (1951) for a cylinder of diameter 0.04 inserted into the base flow and stability computations: (*a*) the eigenvalue spectrum with full-amplitude volume force (cf. figure 10*b*); (*b*) the growth rate of the global mode using a reduced amplitude of the force: the leading mode ($-\circ-$), the second mode ($-\square-$), and the movement for the leading mode predicted from the sensitivity distribution in figure 9 ($-\cdot-$).

mode are shown in figure 11(*b*), together with the prediction from the sensitivity distribution. It is seen that the leading mode follows the predicted behaviour very well at lowest forcing amplitudes, but starts to deviate at $F/F_0 \approx 0.05$, whereafter the dependence on the forcing amplitude becomes nonlinear. Thus, beyond this point, when forcing at this downstream position, we should not expect the sensitivity map to be valid. The first mode switching occurs when $F/F_0 \approx 0.15$ which, based on estimates for drag in creeping flow (the first tem in the Lamb–Oseen expansion, in e.g. Zdravkovich 1997), corresponds to a cylinder of diameter 0.002.

The results show that a small cylinder can be used as a control device in the upstream sensitivity region. In the downstream sensitivity region however, control seems to be difficult, since, depending on the forcing position, several modes are sensitive and their sensitivity is generally not linear with respect to the forcing. The instability can completely change its character due to the insertion of the tiny cylinder. So, even if control could not be established in the downstream region, it is by no means less dynamically important than the upstream region. In fact, changes downstream have a strikingly large influence on the linear dynamics of the flow, in the light of the results presented in both this and previous sections.

6. Discussion

This work deals with analysis and control of wake flow dynamics, in particular the dynamically important spatial regions for globally unstable co-flow wakes. Such wavemaker regions can be sought e.g. in terms of maximal sensitivity to structural perturbations (Giannetti & Luchini 2007), to base-flow modifications (Marquet *et al.* 2008), to volume forcing (Pralits *et al.* 2010) or to specific means of control such as a small control cylinder (Hill 1992). Furthermore, in the local method of approximating linear global modes, the term wavemaker denotes the streamwise location of the complex saddle point, which imposes its absolute frequency in the global oscillation (Huerre & Monkewitz 1990).

https://doi.org/10.1017/jfm.2012.156 Published online by Cambridge University Press

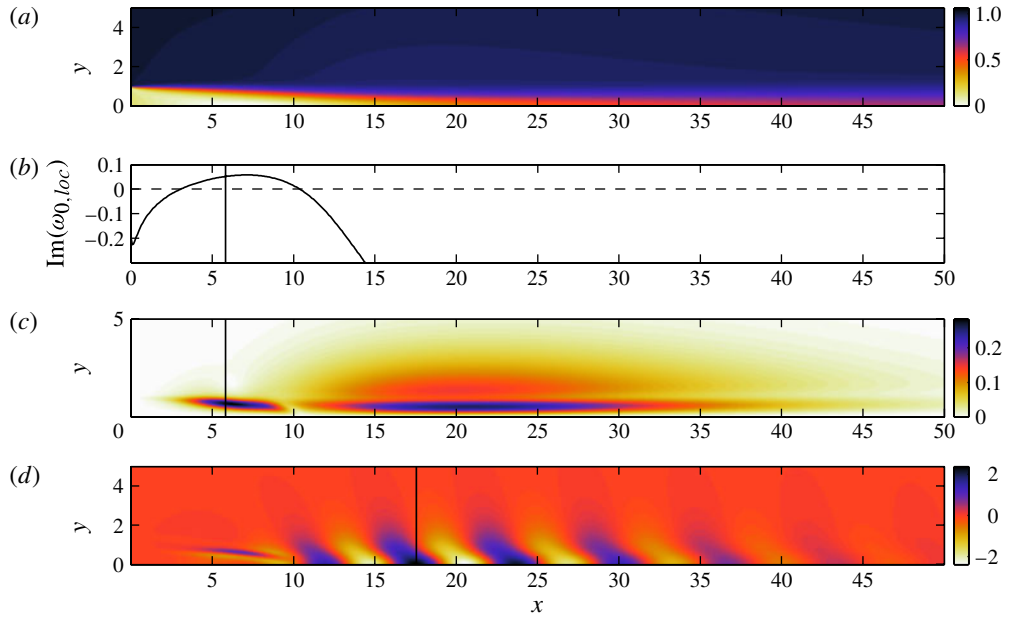


FIGURE 12. (Colour online) Summary of some main characteristics for the wake at $Re = 398$, $h = 9$, $\Lambda^{-1} = -1.32$: (*a*) base flow; (*b*) absolute growth rate from the local linear analysis; (*c*) sensitivity to structural perturbations (global linear analysis); (*d*) sensitivity to modifications of the streamwise base-flow velocity (global linear analysis).

The previous studies on cylinder wakes at low Reynolds numbers have found one clearly dominating region close to the cylinder, with only minor changes in the location depending on the definition of the 'wavemaker'. However, the present work shows that for co-flow wakes at high Reynolds number, there are two streamwise separated regions, both influencing the wake dynamics in different ways.

Figure 12 summarizes the linear results for a weakly confined co-flow wake at $Re = 398$: the base flow is depicted in figure 12(*a*), the absolute growth rate from local analysis in figure 12(*b*), the structural sensitivity to perturbations from global analysis in figure 12(*c*), and the sensitivity to base-flow modifications from global analysis in figure 12(*d*). This figure will be explained and discussed in detail below.

First, in figure 12(*c*) it is seen that the linear structural sensitivity for weakly confined (here termed unconfined) co-flow wakes at $Re \approx 400$ shows two distinct regions of high sensitivity, which are referred to as the upstream region and the downstream region, respectively. The sensitivity to perturbations in the u-momentum equations is depicted here; the sensitivity to perturbations in the v-momentum equation has a similar streamwise distribution.

The upstream region is in the near field of the wake ($x < 10$), as is normal for wake flows. The streamwise location of the saddle point found from local analysis, the 'local wavemaker' ($x = 5.8$, vertical line in figure 12*b*), coincides almost perfectly with the maximum amplitude of the structural sensitivity for u-momentum perturbations ($x = 6.2$, vertical line in figure 12*c*). The local linear frequency prediction ($\omega_0 = 0.74 + 0.046\mathrm{i}$) is in rather good agreement with the global linear one ($\omega_0 = 0.78 + 0.033\mathrm{i}$), also indicating that the frequency of the mode is determined in this region. Furthermore, the results on control by small cylinder in § 5.2 showed

https://doi.org/10.1017/jfm.2012.156 Published online by Cambridge University Press

that the global mode can be stabilized by placing the cylinder in the shear layer at $x < 10$. A similar 'wavemaker' region appears for confined and unconfined wakes in the present work, and for wakes at lower Re, and is similar to the results for cylinder wakes in previous works.

At first sight, the upstream sensitivity region seems to satisfy all the criteria that we would associate with a wavemaker region. What is then the role of the second, downstream high-sensitivity region?

This second region of high structural sensitivity only appears for weakly confined wakes at $Re > 100$. It is more elongated and extends until $x \approx 50$ in the streamwise direction, and also higher up in the free stream in the vertical direction, up to $y \approx 5$ (figure 3*b*). The sensitivity to generic base-flow modifications shows a spatially oscillating pattern inside the downstream region (figure 12*d*); if the base flow is modified at a certain spatial position, then the global mode is stabilized or destabilized depending on the streamwise coordinate of the modification. The eigenvalue changes considerably more when the base flow is modified in the downstream region than in the upstream region, and the maximal sensitivity to base-flow modifications is found at $x = 17.5$ (vertical line in figure 12*d*). The sensitivity to a volume force is also non-vanishing downstream with the familiar oscillatory pattern (for a second wake introduced in appendix B for comparison, the sensitivity to volume forcing is also stronger downstream than upstream). When a control cylinder with diameter 0.04 is placed in the downstream region, the result is a destabilization of several global modes. The spectra are then similar to the spectra with a large generic base-flow modification (appendix B).

It is legitimate to ask the following questions: If the frequency of the unperturbed flow seems to be dictated upstream, why is the flow sensitive to base-flow modifications downstream, and why does a small cylinder far downstream have such a large impact on the flow? After all, this flow is shown to be convectively unstable at $x > 10$ (figure 12*b*, together with the fact that no other unstable saddle points were found in the local analysis), so why would any effect travel upstream and change the frequency in the absolutely unstable region?

The proposed explanation of the cylinder effect is similar to edge tones in a free shear layer (Hussain & Zaman 1978). It is known that a hot wire can create additional frequencies in shear-layer experiments, and that these 'tones' depend on the placement of the hot-wire probe. The oscillations creating the tones occur in the region between the inlet and the hot-wire probe, and lead to frequency jumps in the response when the hot wire is traversed in the streamwise direction. Further, the amplitude of each fundamental tone grows initially, then decays, and is replaced by another fundamental tone (Hussain & Zaman 1978). This is very similar to the spectra as a function of cylinder position in the present work (figure 10). An unconfined co-flow wake at $Re = 400$ has a strong advection, and the wake in the present work is also slightly accelerated by the slow development towards a parabolic profile. It is thus possible that the wake acts as a shear layer with an appropriate forcing. It should be noted that both edge tones, and global modes in cavities exploiting the same mechanism (e.g. Rowley, Colonius & Basu 2002), are usually discussed in the context of compressible flows. However, the same feedback mechanism has been observed for global modes in a smooth incompressible cavity (Åkervik *et al.* 2007). Downstream travelling waves reflected back from the downstream edge of the cavity were evident in the pressure trace of the optimal initial condition, and the global spectrum was also seen to be dependent on the cavity length (Åkervik 2011, personal communication).

https://doi.org/10.1017/jfm.2012.156 Published online by Cambridge University Press

Both phenomena – the oscillating sensitivity distributions for small forcing, and the cascade of modes dependent on the position of the control cylinder – seem to be connected to the strong advection. The sensitivity distributions also show that the flow is very sensitive to changes in base-flow advection downstream (figure 6*b*). Let us assume that a tiny amount of the global mode is always reflected upstream by e.g. pressure feedback. For small changes in advection (local deceleration or acceleration), this reflected part can be either in phase or out of phase with the 'true mode' at or upstream of the position of the 'true wavemaker', at the time of the instantaneous reflection. Thus, it can have either destructive or constructive interference with the wavemaker.

If the reflection is strong enough (corresponding to a large base-flow modification), this mechanism similar to cavity flows dominates the absolute instability with the generation of new modes as a result. The effect can also be coupled with a reflection from the inlet. There is always a solid boundary present at the inlet, either through a splitter plate between the flow streams (physical effect) or through a zero disturbance condition at the wake inlet (numerical effect), the latter case if no extensional regions as in the present work (described in appendix A) are applied.

Hence, two different regions have been identified for a globally unstable flow with a strong advection. There is an upstream 'wavemaker' region where the frequency is dictated, when the flow behaves more like an oscillator. There is also a downstream region, where the flow can be very easily perturbed. A broad high-sensitivity region can be a demonstration of non-normality of the flow, as has been indicated but not explicitly shown previously (e.g. Chomaz 2005). What is remarkable is that this wake flow can transport information from the perturbation source upstream, acting like an 'inverse noise amplifier' and challenging the concepts of absolute and convective instability. However, this might not be as surprising as it sounds, if the reason is a pressure feedback similar to cavity flows, since the pressure feedback is clearly a non-local mechanism.

The sensitivity to conditions downstream should have not only physical, but also numerical consequences. The impact on the numerical solution of the problem is the high resolution needed inside the whole region of high sensitivity to base-flow modifications. This concerns the resolution of both the computed base flow and the 'apparent base flow' in the stability problem, i.e. the resolution of the global-mode computation. Also the relatively high structural sensitivity shows that the global mode must be well-resolved downstream. This is also a major difference from previous wavemaker results for the cylinder flow. While the wakes at lower Reynolds numbers only require high resolution close to the inlet, the co-flow wakes at $Re \approx 400$ must be well-resolved inside a long region downstream. The need of increasing streamwise resolution is counterintuitive, since the flow becomes more parallel for higher Re, but nevertheless was clearly observed during the previous study of Tammisola *et al.* (2011). Here, it should be stressed that all flows and their sensitivities in the present work have gone through careful studies of resolution and boundary condition independence, described in appendix A.

Although the observations in the present work are interesting from a fundamental point of view, a definite next step is to see whether and to what extent they carry over to a nonlinear setup. Although the linear spectrum is very sensitive to downstream forcing, there always seems to be at least one linear mode available to start the initial growth process, and the shape and frequency of the final nonlinear oscillation need not be as sensitive. Only a further study by nonlinear simulations and/or experiments can answer this question. There is no conclusive evidence of edge tones for wake experiments, although have been suggested to be seen by e.g. Kovasznay (1949). Periodic minima and maxima of the vortex formation length, a quantity inversely

https://doi.org/10.1017/jfm.2012.156 Published online by Cambridge University Press

proportional to maximum of u_{rms} (Williamson 1996), are reported also for a cylinder wake at $Re \approx 750$ in Unal & Rockwell (1987), when a splitter plate is traversed in the streamwise direction in a cylinder wake. At low Reynolds numbers ($Re \approx 140$), no such effects were seen. Co-flow wakes could turn out to be a suitable flow case for such studies.

In previous work with cylinder flows at high Re, confined wakes had more narrow spectral distributions than unconfined wakes (e.g. Richter & Naudascher 1976). The randomness in the downstream sensitivity for unconfined wakes seen here, that was completely absent for the confined wake, could contribute to the appearance of a broader spectrum.

7. Conclusions

Passive control and dynamically important regions have been studied for self-sustained oscillations in wake flows. Theoretical sensitivity maps were computed based on the assumption of small base-flow modifications. At higher Reynolds number and weak confinement ($h = 9$, $Re = 398$), there are two streamwise separated regions of high sensitivity.

(i) The upstream sensitivity region behaves like a wavemaker in the classical sense. The global mode can be stabilized in this region, and it is robust in terms of passive control. Local analysis (valid for weakly non-parallel flows) finds a saddle point in the point of maximal amplitude of structural sensitivity. The frequency of this saddle point is reasonably close to the linear global frequency.

(ii) The downstream sensitivity region destroys the robustness of the global mode. The sensitivity of the leading global mode to base-flow modifications and volume forcing alternates between positive and negative values, depending on the streamwise coordinate of the modification. The theory indicates that if a tiny control cylinder were traversed in the streamwise direction, the growth rate would oscillate as a function of cylinder position. It is shown that if a finite but small control cylinder is used, the flow behaves instead like a cavity, with mode-switching depending on the coordinate of the control cylinder (cf. changing the length of the cavity).

(iii) The mechanism for the downstream sensitivity is suggested to be an incompressible pressure feedback. By this mechanism, the global mode can be slightly reflected upstream, and the reflection can be in phase or out of phase with the actual wavemaker (upstream region). Note that such an upstream propagation would not be detected by a local stability analysis.

(iv) The upstream region is appropriate for control, while one should carefully avoid disturbing the wake inside the downstream sensitivity region to achieve controllability. Disturbances should be carefully eliminated there, both from inadequate numerical resolution, as well as numerical and experimental boundary conditions.

Acknowledgements

Following people are especially acknowledged for sharing their thoughts around the sensitivities: F. Lundell, P. Schlatter, L. Brandt, J. Pralits, M. Ilak. M. Juniper is acknowledged for help and advice regarding the local analysis. The support from the European Union FP6 Project Ecotarget and the Swedish Research Council, Linné FLOW Centre is gratefully acknowledged.

https://doi.org/10.1017/jfm.2012.156 Published online by Cambridge University Press

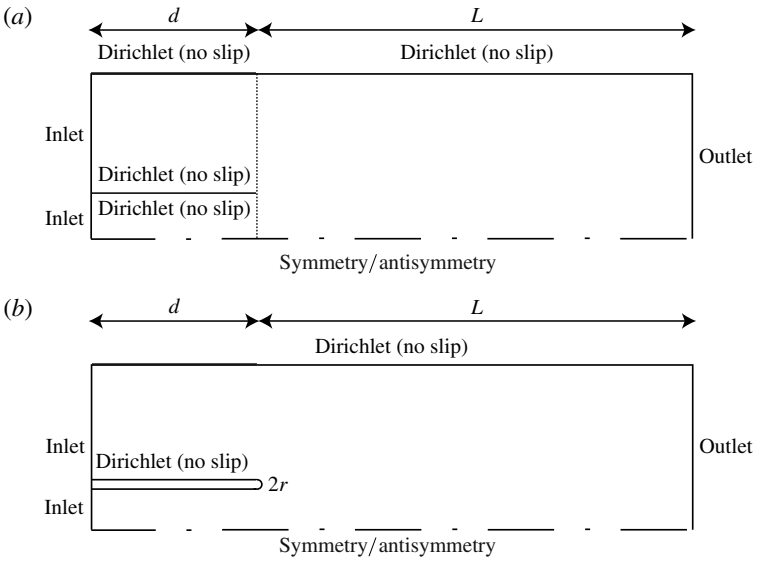


FIGURE 13. Illustration of the two computational domains used in this study: (*a*) inlet profile at $x = 0$ combined with a damping region at $-d < x < 0$ (all results except appendix B); (*b*) inlet profile at $x = -d = -1$ combined with a splitter plate at $-d < x < 0$ (appendix B).

Appendix A. Numerical treatment

The first numerical setup (figure 13*a*) utilizes a damping-region concept, also used in Tammisola *et al.* (2011). In this setup, the base flow is computed in the region $x > 0$, and the inlet profile shown in figure 1 is set at $x = 0$. In the stability problem however, the numerical domain is continued to the region $x < 0$, where we set a no-slip condition between the two fluid streams, resembling an 'infinitely thin plate'. The base flow is kept equal to the inlet profile in this region. The purpose of this 'damping region' of length d is only to let the global mode decay more smoothly, and avoid spurious reflections from the inlet, without altering the base flow. Then, the length d can be varied to test the dependence of the global mode on the inlet boundary condition, and L the dependence for the outlet boundary condition.

The sensitivities are also seen to be essentially invariant with respect to the numerical discretization used, the resolution and the boundary conditions of the stability problem. The boundary conditions used were the following. At the inlet, a homogeneous Dirichlet condition is set (zero disturbance):

$$\hat{u}(-d, y) = \hat{v}(-d, y) = 0. \tag{A 1}$$

At the walls we have a no-slip condition:

$$\hat{u} = \hat{v} = 0. \tag{A 2}$$

At the centreline antisymmetry is imposed (since all the unstable modes were known to be antisymmetric):

$$\hat{u}(x, 0) = \frac{\partial \hat{v}}{\partial y}(x, 0) = \hat{p}(x, 0) = 0. \tag{A 3}$$

https://doi.org/10.1017/jfm.2012.156 Published online by Cambridge University Press

Base flow code	Stability code	L	d	md_1	md_2	max(S_{adv})	Position of max(S_{adv})
Comsol	Comsol	250	10	0.07	0.18	3.7437	(19.41, 0.4000)
Nek5000	Comsol	250	20	0.07	0.2	4.1940	(19.50, 0.4000)
Comsol	Comsol	160	10	0.07	0.18	3.7392	(19.41, 0.4000)
Comsol	Comsol	160	110	0.07	0.18	3.8430	(19.42, 0.4000)
Comsol	Comsol	95	10	0.04	0.14	3.7995	(19.35, 0.4000)

TABLE 1. The maximal value of S_{adv} and its location in space for different numerical configurations. md_1 denotes the maximal grid point distance in the region $0 < x < 50, 0 < y < 1$, and md_2 the maximal grid point distance in the region $0 < x < 50, 1 < y < 10$.

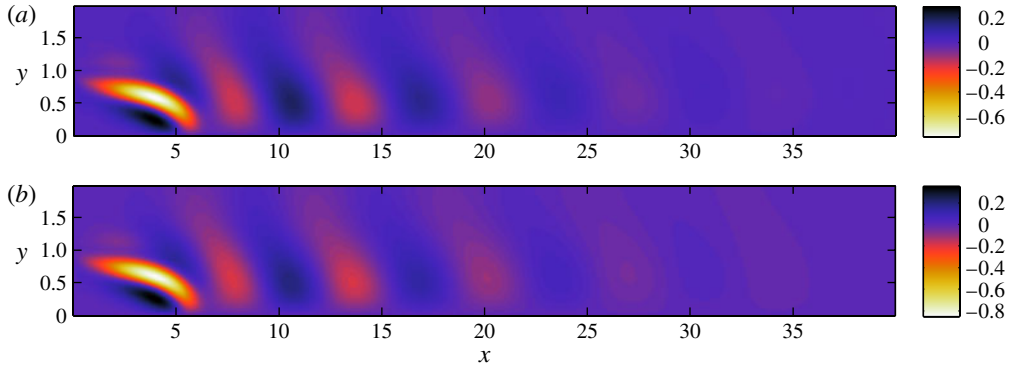


FIGURE 14. (Colour online) S_V for the same base flow, with stability computed using: (*a*) FLUPACK; (*b*) Comsol.

At the outlet, a stress-free condition was chosen, although the tests showed that the choice was not important here:

$$-\hat{p} + \frac{1}{Re}\frac{\partial \hat{u}}{\partial x} = \frac{\partial \hat{v}}{\partial x} = 0. \tag{A 4}$$

In table 1, the numerical accuracy is quantified by the maximum value of the magnitude of the advective part of the sensitivity to base-flow modifications (S_{adv}). This is the part that contains most of the oscillating behaviour. Two different codes are used for calculating the base flow: the Nek5000 spectral-element code and the Comsol Multiphysics finite-element code. In the Nek5000 simulation, the inlet profile needs to be slightly smoothed, but even this is seen to have a very minor effect on the results. For the stability, we use mainly Comsol Multiphysics, which has been verified against our own spectral software FLUPACK in Tammisola *et al.* (2011). FLUPACK has problems in resolving the sensitivities very accurately at high Reynolds numbers, due to the point distribution (Gauss–Lobatto–Chebyshev points). Therefore, we perform a verification comparing FLUPACK and Comsol at $Re = 158$, and with probably too short a domain ($L = 50$) to meet the resolution requirements. Despite the short domain, the oscillatory pattern is still strikingly similar to the one obtained from Comsol with a long domain (S_V for both shown in figure 14).

https://doi.org/10.1017/jfm.2012.156 Published online by Cambridge University Press

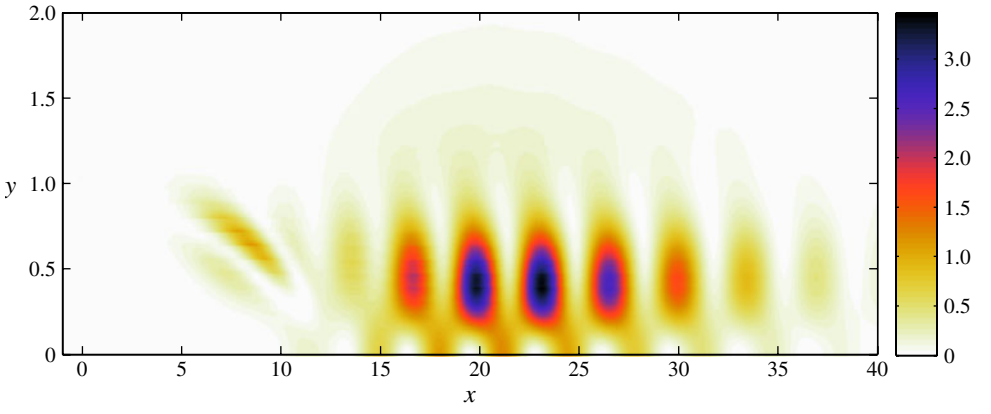


FIGURE 15. (Colour online) The change to generic changes in base-flow advection, S_{adv}, for the round-edged plate.

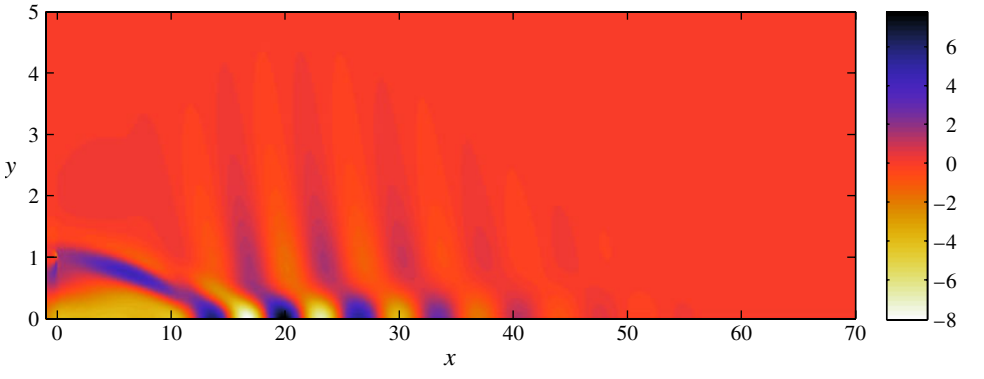


FIGURE 16. (Colour online) Sensitivity to a steady volume force in the streamwise direction (positive forcing direction aligned with unit vector [1, 0]), for the round-edged plate case. The region $y > 0$ is shown; the sensitivity at $y < 0$ is the mirror image.

Appendix B. Results for a round-edged plate with a boundary layer before the inlet

Here, the sensitivity is computed with a more realistic inflow model. The fluid streams are separated prior the wake (at $-d < x < 0$) by a round-edged plate of finite thickness (figure 13*b*). The base-flow profile is allowed to develop prior to the wake and develop thin boundary layers at $x < 0$. Since boundary layers have a damping effect on the stability, the development region has to be kept rather short at these Reynolds numbers. In this section, results are presented for $d = 1$.

In the following, the round-edged plate setup will be called setup B, and the setup used in the main body of the paper and appendix A (described in appendix A) will be called setup A.

The advective part of the sensitivity to base-flow modifications for setup B is shown in figure 15, and shows an even stronger oscillatory pattern than for setup A shown previously (figure 6). The same is true for the sensitivity to a steady volume force shown for setup B in figure 16 (compared to the one for setup A shown in figure 8),

https://doi.org/10.1017/jfm.2012.156 Published online by Cambridge University Press

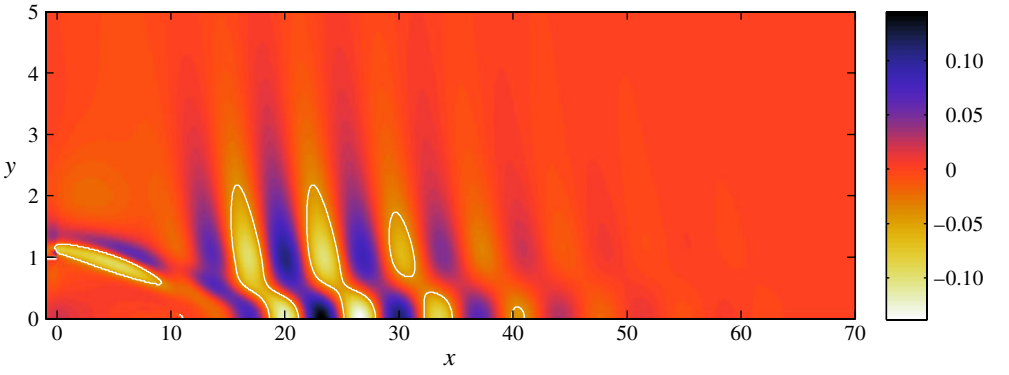


FIGURE 17. (Colour online) Sensitivity to a control cylinder of diameter 0.02 for a round-edged plate. Region where stabilization is predicted is marked by the white contours.

and the sensitivity to a control cylinder for setup B in figure 17 (compared to figure 9 for setup A). Since the oscillatory patterns appear for both setups, we have now verified that the inlet modelling used for setup A does not cause the oscillations. Together with the tests of different discretizations, streamwise boundary conditions and resolutions presented in appendix A, it can be concluded that the oscillations most probably have a physical origin.

The verification of the sensitivity to base-flow modification is again performed by modifying the actual base flow by the distribution (4.1) at different positions x_{mod}, and recomputing the direct global modes in all cases. The result is compared to the prediction from adjoint-based sensitivity distributions, for different amplitudes of the base-flow modification; for setup B, both small and larger amplitudes were tested. The change in the most unstable mode with a base-flow modification of a small amplitude is shown in figures 18(*a*) (growth rate) and 18(*b*) (frequency). These small-amplitude modifications agree well with the theory. However, when the modification amplitude increases to $A = 0.02$ (figure 18*c*,*d*), which is 10 % of the maximal vertical velocity, the solution starts to deviate from the theoretical curve. For $A = 0.05$ and $A = 0.1$ the original mode is soon replaced by new modes. Every 'jump' in the frequency curve in figure 18(*d*) indicates that a new mode has taken over as the most unstable mode.

Appendix C. Linearized drag model for the control cylinder

The dimensional drag force per unit spanwise length for the control cylinder is expressed in tensor form as

$$D^*_{F,i} = -\tfrac{1}{2} C_{D,tot} \rho^* |U^*_{tot}| D^* U^*_{tot,i}, \tag{C 1}$$

where ρ^* is the density, D the diameter of the control cylinder, $C_{D,tot}$ the drag coefficient of the control cylinder, and U^*_{tot} the total velocity field, and in non-dimensional form

$$D_{F,i} = -\frac{D^*_{F,i}}{\tfrac{1}{2}\rho^* U^{*2}_2 \; h^*_1} = -C_{D,tot} |\bar{U}_{tot}| D U_{tot,i}. \tag{C 2}$$

Let us now divide the total quantities (with subscript 'tot') into a steady and unsteady linear part (uppercase versus lowercase letters): $C_{D,tot} = C_D + c_D$, $U_{tot,i} = U_i + u_i$.

https://doi.org/10.1017/jfm.2012.156 Published online by Cambridge University Press

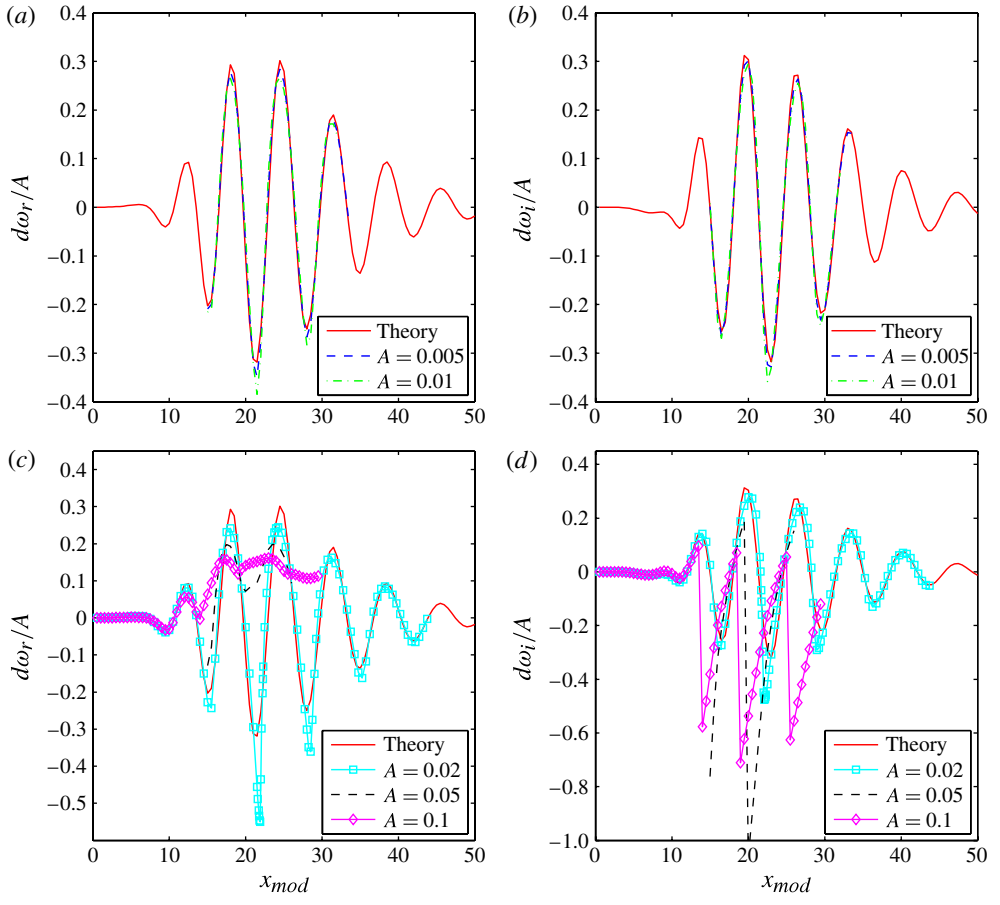


FIGURE 18. (Colour online) The change in the frequency and the growth rate of the most unstable eigenvalue with modifications of different amplitude along the line $y = 0.5$ (varying x_{mod}): (*a*) frequency, small-amplitude modifications; (*b*) growth rate, small-amplitude modifications; (*c*) frequency, large-amplitude modifications; (*d*) growth rate, large-amplitude modifications.

Then we get

$$D_{F,i} = -D\left(C_D|\bar{U}_{tot}|U_i + C_D|\bar{U}_{tot}|u_i + c_D|\bar{U}_{tot}|U_i + c_D|\bar{U}_{tot}|u_i\right). \tag{C 3}$$

The last term is neglected in the linear approximation. Further, we need to linearize $|U_{tot}|$:

$$\begin{aligned} |\bar{U}_{tot}| &= \sqrt{(U+u)^2 + (V+v)^2} \\ &\approx \sqrt{U^2+V^2} + \tfrac{1}{2}\left[U^2+V^2\right]^{(-1/2)}(2Uu + 2Vv) \\ &= |\bar{U}| + \frac{(Uu+Vv)}{|\bar{U}|}, \end{aligned} \tag{C 4}$$

https://doi.org/10.1017/jfm.2012.156 Published online by Cambridge University Press

which leads to

$$\begin{aligned} D_{F,i} &\approx -Dg(C_D|\bar{U}_{tot}|U_i + C_D|\bar{U}_{tot}|u_i + c_D|\bar{U}_{tot}|U_i) \\ &\approx -D\Bigg(C_D|\bar{U}|U_i + C_D\frac{(Uu+Vv)}{|\bar{U}|}U_i + C_D|\bar{U}|u_i \\ &\quad + C_D\frac{(Uu+Vv)}{|\bar{U}|}u_i + c_D|\bar{U}|U_i + c_D\frac{(Uu+Vv)}{|\bar{U}|}U_i\Bigg) \\ &\approx -D\left(C_D|\bar{U}|U_i + C_D\frac{(Uu+Vv)}{|\bar{U}|}U_i + C_D|\bar{U}|u_i + c_D|\bar{U}|U_i\right). \end{aligned} \tag{C 5}$$

Now it remains to find C_D and c_D, by linearizing an appropriate expression for $C_{D,tot}$. An empirical expression for a cylinder in a uniform stream in good agreement with experiments for $5 < Re < 100$ is, according to Zdravkovich (1997), found from Imai (1951) as:

$$C_{D,tot} = \left(0.707 + \frac{3.42}{\sqrt{Re_c}}\right)^2, \tag{C 6}$$

where Re_c is the cylinder Reynolds number. For the flow case in the present work this is rewritten according to

$$C_{D,tot} = \left(0.707 + \frac{3.42}{\sqrt{Re|\bar{U}_{tot}|D}}\right)^2. \tag{C 7}$$

By inserting (C 5) into this and developing, we get

$$\begin{aligned} C_{D,tot} &= \left(0.707 + \frac{3.42}{\sqrt{Re|\bar{U}_{tot}|D}}\right)^2 \\ &\approx \left(0.707 + \frac{3.42}{\sqrt{Re|\bar{U}|D}}\right)^2 \\ &\quad + 2\left(0.707 + \frac{3.42}{\sqrt{Re|\bar{U}|D}}\right)\frac{3.42}{\sqrt{ReD}}\left[-\frac{1}{2}|\bar{U}|^{-3/2}\frac{(Uu+Vv)}{|\bar{U}|}\right] \\ &= \left(0.707 + \frac{3.42}{\sqrt{Re|\bar{U}|D}}\right)^2 \\ &\quad - \frac{3.42}{\sqrt{Re|\bar{U}|D}}\left(0.707 + \frac{3.42}{\sqrt{Re|\bar{U}|D}}\right)\left[\frac{(Uu+Vv)}{|\bar{U}|^2}\right]. \end{aligned} \tag{C 8}$$

This can be written in a simple form by introducing functions varying with the local velocity, $\alpha = 3.42/\sqrt{Re|\bar{U}|D}$ and $\beta = (0.707 + \alpha)$:

$$C_D = \beta^2 \tag{C 9}$$

and

$$c_D = -\alpha\beta\frac{(Uu+Vv)}{|\bar{U}|^2}. \tag{C 10}$$

https://doi.org/10.1017/jfm.2012.156 Published online by Cambridge University Press

Now we can identify components and divide the drag into steady and unsteady parts as

$$D_{F(steady),i} = -D\beta^2|\bar{U}|U_i, \tag{C 11}$$

$$\begin{aligned} D_{F(unsteady)} &= -D\left[\beta^2 U_i\frac{(Uu+Vv)}{|\bar{U}|^2} + \beta^2|\bar{U}|u_i - \alpha\beta|\bar{U}|U_i\frac{(Uu+Vv)}{|\bar{U}|^2}\right] \\ &= -D(\beta^2 - \alpha\beta|\bar{U}|)U_i\frac{(Uu+Vv)}{|\bar{U}|^2} - D\beta^2|\bar{U}|u_i. \end{aligned} \tag{C 12}$$

Now when the components of the linearized force have been obtained, they should be considered as point forces in the steady equations and linearized momentum equations, respectively (to obtain the correct total force on the flow). The sensitivities can now be obtained e.g. from the expressions in Pralits *et al.* (2010), repeated again for convenience.

For an unsteady force of the form $f = \delta(x - x_0)(y - y_0)m_{ij}u_j$, the sensitivity is given by

$$\delta\omega = u_i^+ m_{ij}u_j, \tag{C 13}$$

and for a steady force of the form $F = \delta(x - x_0)(y - y_0)M_{ij}u_j$

$$\delta\omega = U_i^+ M_{ij}U_j. \tag{C 14}$$

The normalization can be skipped, since our adjoints are already appropriately normalized, according to (2.12).

The above expressions give

$$M_{UU} = -D\beta^2|\bar{U}|, \quad M_{VV} = -D\beta^2|\bar{U}|, \quad M_{UV} = M_{VU} = 0, \tag{C 15}$$

$$\begin{aligned} m_{uu} &= -D\left(\beta^2 - \alpha\beta|\bar{U}|\right)U^2/|\bar{U}|^2 + D\beta^2|\bar{U}|, \\ m_{uv} &= -D\left(\beta^2 - \alpha\beta|\bar{U}|\right)UV/|\bar{U}|^2, \end{aligned} \tag{C 16}$$

$$\begin{aligned} m_{vu} &= -D\left(\beta^2 - \alpha\beta|\bar{U}|\right)UV/|\bar{U}|^2, \\ m_{vv} &= -D\left(\beta^2 - \alpha\beta|\bar{U}|\right)V^2/|\bar{U}|^2 + D\beta^2|\bar{U}|. \end{aligned} \tag{C 17}$$

REFERENCES

Åkervik, E. 2011 Personal communication.

Åkervik, E., Hœpffner, J., Ehrenstein, U. & Henningson, D. S. 2007 Optimal growth, model reduction and control in a separated boundary-layer flow using global eigenmodes. *J. Fluid Mech.* **579**, 305–314.

Bearman, P. W. & Zdravkovich, M. M. 1978 Flow around a circular cylinder near a plane boundary. *J. Fluid Mech.* **89**, 33–47.

Chomaz, J.-M. 2005 Global instabilities in spatially developing flows: non-normality and nonlinearity. *Annu. Rev. Fluid Mech.* **37**, 357–392.

Fey, U., König, M. & Eckelmann, H. 1998 A new Strouhal–Reynolds-number relationship for the circular cylinder in the range $47 < Re < 2 \times 10^5$. *Phys. Fluids* **10** (7), 1–3.

Filon, L. N. G. 1926 The forces on a cylinder in a stream of viscous fluid. *Proc. R. Soc. Lond.* A **113**, 7–27.

Giannetti, F. & Luchini, P. 2007 Structural sensitivity of the first instability of the cylinder wake. *J. Fluid Mech.* **581**, 167–197.

Hill, D. 1992 A theoretical approach for analyzing the restabilization of wakes. *AIAA Paper* 92–0067.

https://doi.org/10.1017/jfm.2012.156 Published online by Cambridge University Press

HUERRE, P. & MONKEWITZ, P. A. 1990 Local and global instabilities in spatially developing flows. *Annu. Rev. Fluid Mech.* **22**, 473–537.

HUSSAIN, A. K. M. F. & ZAMAN, Q. 1978 The free shear layer tone phenomenon and probe interference. *J. Fluid Mech.* **87** (2), 349–383.

IMAI, I. 1951 On the asymptotic behaviour of viscous fluid flow at a great distance from a cylindrical body, with special reference to Filon's paradox. *Proc. R. Soc. Lond.* A **208**, 487–516.

JUNIPER, M. P. 2006 The effect of confinement on the stability of two-dimensional shear flows. *J. Fluid Mech.* **565**, 171–195.

JUNIPER, M., TAMMISOLA, O. & LUNDELL, F. 2011 The local and global stability of confined planar wakes at intermediate Reynolds number. *J. Fluid Mech.* **686**, 218–238.

KOVASZNAY, L. 1949 Hot-wire investigation of the wake behind cylinders at low Reynolds numbers. *Proc. R. Soc. Lond.* A **198** (1053), 174–190.

MARQUET, O., SIPP, D. & JACQUIN, L. 2008 Sensitivity analysis and passive control of cylinder flow. *J. Fluid Mech.* **615**, 221–252.

PRALITS, J., BRANDT, L. & GIANNETTI, F. 2010 Instability and sensitivity of the flow around a rotating circular cylinder. *J. Fluid Mech.* **650**, 513–536.

REES, S. J. & JUNIPER, M. P. 2010 The effect of confinement on the stability of viscous planar jets and wakes. *J. Fluid Mech.* **656**, 309–336.

RICHTER, A. & NAUDASCHER, E. 1976 Fluctuating forces on a rigid circular cylinder in confined flow. *J. Fluid Mech.* **78**, 561–576.

ROWLEY, C. W., COLONIUS, T. & BASU, A. J. 2002 On self-sustained oscillations in two-dimensional compressible flow over rectangular cavities. *J. Fluid Mech.* **455**, 315–346.

STRYKOWSKI, P. J. & SREENIVASAN, K. R. 1990 On the formation and suppression of vortex 'shedding' at low Reynolds numbers. *J. Fluid Mech.* **218**, 71–107.

TAMMISOLA, O., LUNDELL, F., SCHLATTER, P., WEHRFRITZ, A. & SÖDERBERG, L. D. 2011 Global linear and nonlinear stability of viscous confined plane wakes with co-flow. *J. Fluid Mech.* **675**, 397–434.

UNAL, M. F. & ROCKWELL, D. 1987 On vortex formation from a cylinder. Part 2. Control by splitter-plate interference. *J. Fluid Mech.* **190**, 513–529.

WILLIAMSON, C. H. K. 1996 Vortex dynamics in the cylinder wake. *Annu. Rev. Fluid Mech.* **28**, 477–539.

ZDRAVKOVICH, M. M. 1997 *Flow Around Circular Cylinders,* vol. 1. Oxford University Press.

ZEBIB, A. 1987 Stability of viscous flow past a circular cylinder. *J. Engng Maths* **21** (2), 155–165.

https://doi.org/10.1017/jfm.2012.156 Published online by Cambridge University Press